Bioactive Materials 3 (2018) 255–266

Contents lists available at ScienceDirect

Bioactive Materials

journal homepage: http://www.keaipublishing.com/en/journals/bioactive-materials/

Starch based nanofibrous scaffolds for wound healing applications

Vijaya Sadashiv Waghmare [a], Pallavi Ravindra Wadke [a], Sathish Dyawanapelly [a, b], Aparna Deshpande [c], Ratnesh Jain [b, **], Prajakta Dandekar [a, *]

[a] Department of Pharmaceutical Sciences and Technology, Institute of Chemical Technology, Matunga, Mumbai 400019, India
[b] Department of Chemical Engineering, Institute of Chemical Technology, Matunga, Mumbai 400019, India
[c] Department of Physics, Indian Institute of Science Education and Research (IISER), Pashan, Pune 411008, India

ARTICLE INFO

Article history:
Received 21 June 2017
Received in revised form
3 November 2017
Accepted 21 November 2017
Available online 26 November 2017

Keywords:
Starch
Nanofibers
Electrospinning
Scaffold
Wound healing

ABSTRACT

Starch is an attractive polymer for wound healing applications because of its wide availability, low cost, biocompatibility, biodegradability and wound-healing property. Here, we have fabricated starch-based nanofibrous scaffolds by electrospinning for wound healing applications. The diameter of the optimized nanofibers was determined by field emission scanning electron microscopy (FE-SEM) and was found to be in the range of 110–300 nm. The mechanical strength (0.5–0.8 MPa) of the nanofibrous scaffolds was attuned using polyvinyl alcohol (plasticizer) and glutaraldehyde (crosslinking agent), to impart them with sufficient durability for skin tissue engineering. Absence of negative interactions between the polymers was confirmed by Attenuated Total Reflectance-Fourier Transform Infrared Spectroscopy (ATR-FTIR), differential scanning microscopy (DSC) and thermal gravimetric analysis (TGA). Cellular assays with L929 mouse fibroblast cells indicated the ability of the scaffolds to promote cellular proliferation, without exhibiting any toxic effect to the cells. Thus, the nanofibrous scaffolds demonstrated potential for wound healing applications.

1. Introduction

Tissue engineering is an interdisciplinary biomedical approach that aims to regenerate, reconstruct or repair damaged tissues by supporting the cells with the help of artificial 3D materials [1]. These 3D scaffolds material assist in mimicking the activity of natural extracellular matrix that accommodates the cells in their natural milieu [2]. The cells proliferate and migrate within this matrix to assume their inherent orientation and arrangement. The entire process is governed by the dimension, pore geometry and pore size of the scaffolds, which play a critical role in providing oxygen and nutrient transport to the growing cells. Although various processes have been investigated to develop scaffolds with varying physicochemical properties, the electrospinning technique has proven to be particularly attractive due to its ability to generate scaffolds composed of uniform nanofibers. Moreover, the method offers flexibility to manipulate the fiber dimensions to provide surface area and porosity suitable for diverse biomedical applications. A particularly attractive application is the ability of these nanofibrous scaffolds to simulate the natural extracellular matrix (ECM) and allow adhesion and proliferation of cells seeded on their surface [3]. Besides, the nanofibers provide a surface area to volume ratio and suitable tensile strength to sustain cellular growth. These properties have encouraged increasing employment of this technique in tissue engineering and for fabricating biomedical implants [4]. Despite the simplicity of the process, processing of natural polysaccharides by electrospinning remains a challenging task. The complex chain conformation of polysaccharides and their hydrodynamic responses and repulsive forces, while in solution, negatively influence the spinning efficiency and production of reproducible nanofibers from this class of polymers. In this investigation we have employed electrospinning for producing nanofibrous scaffolds of starch biopolymer. Starch-based biomaterials and it scaffolds have been previously used for several biomedical applications [5]. Starch, as a material by itself, has been explored for wound-healing [6–8]. Also, starch-based scaffolds have been used for adhesion, proliferation, differentiation and regeneration of cells. In recent study, enhanced regeneration of epithelial tissue was

* Corresponding author.
** Corresponding author.
E-mail addresses: rd.jain@ictmumbai.edu.in (R. Jain), pd.jain@ictmumbai.edu.in (P. Dandekar).
Peer review under responsibility of KeAi Communications Co., Ltd.

https://doi.org/10.1016/j.bioactmat.2017.11.006

achieved during wound healing, with the help of collagen, chitosan and starch membrane. Thus, starch-based scaffolds have immense therapeutic significance in wound healing [9]. It has received much attention in drug delivery and other biomedical applications because of its extensive availability, low cost and total composability without generating any hazardous residues. Employment of starch for biomedical functions is also appealing due to its similarity to the native cellular milieu [10]. However certain fundamental properties of starch such as its mechanical properties and moisture sensitivity have to be manipulated to enable its applications in tissue engineering, at par with some commercial expensive polymers [11]. The inherent properties of starch can be altered by with help of polyvinyl alcohol (PVOH), a non-toxic, water soluble, biocompatible, synthetic polymer that can reduce the repulsive forces produced in starch solution and can thus allow electrospinning of its fibers [12]. Another important attribute of starch is its tendency to undergo gelation upon heating, which confers it Non-Newtonian fluid nature. Retrogradation is another characteristic of starch that causes its separation from water, upon cooling, resulting in two different phases [13]. These properties of starch may complicate its electrospinning in the form of aqueous solution, stressing the need to employ a modified solvent system.

In the present work, we report the development of starch-based nanofibrous scaffolds using PVOH as the plasticizer. Electrospun nanofibers of starch-PVOH combinations were successfully developed using hydro-alcoholic solvent for the polymers, for end-application in wound healing. The process was optimized to yield nanofibers with diameters ranging between 110 and 300 nm. The nanofibrous sheet was subsequently cross-linked to enhance its mechanical properties. Evaluation of the optimized nanofibrous scaffolds in cellular assays involving L929 mouse fibroblast cells demonstrated their non-toxicity and their ability to promote cellular proliferation.

2. Materials and methods

2.1. Materials

Potato starch was kindly gifted by Signet Chemical Corporation Pvt. Ltd., Mumbai, India [14]. Absolute ethanol and glutaraldehyde were received from SD fine Chem. Ltd., Mumbai, India. Water soluble PVOH (MW ~ 18,000 g/mol; Degree of hydrolysis = 86.5–89.0 mol %) was purchased from Himedia Laboratories, Mumbai, India. The electrospinning unit, EspinNano-2, was procured from Physics equipment, Chennai, India. Dulbecco's Modified Eagle Medium (DMEM) and EZBlue Cell Assay kit were obtained from Himedia Laboratories, Mumbai, India. The cell line L929 mouse fibroblast was procured from National Centre for Cell Sciences (NCCS), Pune, India. Deionized and double-distilled water (Milli-Q Plus system, Millipore, Bedford, MA, USA) was used in all the experiments.

2.2. Preparation of nanofibers using electrospinning

The electrospinning unit (EspinNano-2, Physics equipment, Chennai, India) was equipped with syringe of 5 mL volume and needles with internal diameter of 0.5 mm. In brief, a blend of starch and PVOH in water was heated up to 70 °C for preparing a homogeneous polymeric solution. Starch to PVOH (S/PVOH) ratio was maintained at 30:70 w/w during the experiments. The spinning dope was prepared at different polymer-blend concentrations of 10%, 12% and 14% w/v using 10% v/v absolute ethanol as the solvent system. Various process parameters were optimized to obtain nanofibers of suitable dimensions. The flow rate was varied between 0.3 mL/h to 0.5 mL/h, while the voltage was varied between 15 and 37 kV. A rotating collector drum covered with aluminum foil was used to collect the ejected fibers, whose distance from the tip of the needle was varied in between 13 and 23 cm.

2.3. Surface morphology

The surface morphology of the nanofibers was studied by Field Emission Scanning Electron Microscopy (UltraPlus Zeiss-4048, Germany). Small pieces of nanofibrous mats were used for the investigation (3 mm × 3 mm). The samples were sputter coated with gold (Quorum Technology, Q150ES, UK) for 30s. The coated samples were mounted over the stubs with the help of carbon tape and analyzed at acceleration voltage of 15 kV, at 0.2 to 0.3 bar, with working distance of 15 cm. The average diameter and standard deviation of fiber was calculated using image analysis software (ImageJ software v1.383, National Institutes of Health, USA). All samples were analyzed in triplicate.

2.4. Crosslinking of nanofibers

The nanofibrous mats were cross-linked to enhance their mechanical property. The prepared mats were compressed on a compression machine (Model MP-15; Technosearch Instruments, Mumbai, India) under a pressure of 10 ton, at room temperature in order to improve their mechanical properties, uniformity and also to minimize the void contents between fibers. Then compressed mats (dimension of 10 mm × 10 mm) were immersed in glutaraldehyde solutions of varying strengths (25%, 15%, 12.5% and 5%v/v; 1 mL) for 12 h. Thereafter, glycine solution (1 mL; 0.02M) was added and kept for 6 h to remove excess glutaraldehyde. The samples were then washed with water, six times, periodically at intervals of 30 min to remove glycine or glutaraldehyde.

2.5. Mechanical strength

The tensile or mechanical strength of the nanofibrous mats was measured using Universal Tensile Machine (UTM) (Tinius Olsen, Model H5KS, USA). Cross-linked scaffolds were cut into sections of dimensions 13.5 cm × 2.5 cm. The resulting scaffolds were mounted between two clamps and stretched at rate of 50 mm/min with an applied load range of 50 N and gauge length of 50 mm. Tensile strength was recorded in triplicate ($n = 3$) at room temperature and average value was calculated.

2.6. Attenuated total reflectance fourier transform infrared spectroscopy (ATR-FTIR)

The presence of functional groups was confirmed by Attenuated Total Reflectance Fourier Transform Infrared Spectroscopy (ATR FTIR; Model-Bruker Alpha platinum FT-IR supported with Opus software). The spectra were obtained between wave numbers 400 to 4000 cm^{-1}. Samples of nanofibrous mats were dehydrated by vacuum drying (45 °C) and then placed over the diamond crystal for analysis. 20 scans were recorded for each spectrum. Smoothing was done wherever necessary to reduce the noise, without loss of any peak. The effect of crosslinking was also studied to study any chemical interaction between the polymers or the amide bond formation during crosslinking.

2.7. Differential scanning calorimetry

Analysis of any possible polymer interaction and the thermal transitions was conducted using Differential Scanning Calorimetry (DSC; Perkin Elmer Model-6, USA). A fixed amount of sample (10 mg) was used throughout the analysis. The weighed samples

were taken into aluminum pans and were hermetically sealed. Empty pan was used as reference. The scans were recorded from 37 °C to 450 °C, at heating rate of 10 °C/min, under nitrogen.

2.8. Thermo gravimetric analysis

The degradation rate of the nanofibrous mats was studied by Thermo Gravimetric analysis (TGA; Perkin Elmer Model-6, USA). The samples were dried at 37 °C for 6 h, prior to analysis. 10 mg of each sample was heated at a constant rate of 10 °C/min. The TGA trace was obtained in the temperature range from 40 to 500 °C, under nitrogen flow rate of 30 mL/min. Graphs of percent weight loss versus temperature were used for interpretation.

2.9. Water uptake

The crosslinked scaffolds of S/PVOH, prepared with different concentrations of the polymer blend, were vacuum dried and immersed in water over period of 15 days. For water uptake study, different mats were used and immersed separately for different time intervals. The water uptake of the mats was calculated on wet and dry basis by using the following Equation (1). The excess water was wiped from the scaffolds before performing the calculations.

$$\text{Water uptake}(\%) = \frac{(Gs - Gi)}{Gi} \times 100 \quad (1)$$

where, *Gi* represents initial dry weight of the nanofibrous mat, and *Gs* is the weight of the nanofibrous mat in wet state [15].

2.10. Cellular proliferation and cytotoxicity studies

Cellular safety and proliferation of the optimized cross-linked scaffolds were evaluated by testing cellular cytotoxicity using EZBlue Cell Assay kit (Himedia Laboratories, Mumbai, India). The cell line used for cytotoxicity assay was L929 mouse fibroblast cell line (ATCC CCL 1). The cells were cultured in 24 well plate in DMEM F12 (Himedia Laboratories, Mumbai, India) supplemented with 10% fetal bovine serum (FBS) (Invitrogen, USA), and 1% Antibiotic-Antimycotic (100 × ; Life Technologies, Mumbai, India) containing Streptomycin, Penicillin and Amphotericin B. The media was replaced every 72–96 h. The cells were trypsinized and cell number was calculated using a haemocytometer. The resulting cell suspension was centrifuged (Remi, Mumbai, India) for 5 min at 20 °C and re-suspended in supplemented media. Each scaffold sample of dimensions 10 mm × 10 mm was sterilized using 70% ethanol and further exposure to UV radiations for 20 min. The scaffolds were then seeded with cells at the density of 1.5×10^5 cells. Cross-linked nanofibrous mats with cells were incubated at 37 °C, with 5% CO_2, with 1 mL of supplemented media in each well. Constructs were evaluated using EZblue blue assay kit at day 1, 3, 5 and 7, post seeding. The medium in the wells containing scaffolds was replaced with medium (1 mL) containing 10% EZBlue blue dye (10% EZBlue blue, 80% media and 10% FBS) and incubated for 3 h. Thereafter, 300 μl of the medium containing EZBlue blue dye was pipette out and the optical density was measured at 570 nm keeping 600 nm as a reference wavelength, using a microplate spectrophotometer (Synergy H1 Model, BioTek instruments, Inc., VT, USA) [16,17]. EZblue blue dye is not toxic to the cells and does not kill the cells to obtain measurements, as in case with 3-(4, 5-dimethylthiazol-2-yl)-2, 5-diphenyl-tetrazolium bromide (MTT). This allows cells to be reused for further investigations, if needed. All the samples were analyzed in triplicates ($n = 3$).

2.11. Statistical analysis

Statistical analyses were performed using one-way ANOVA followed by Bonferroni's post-hoc comparisons tests. A comparison between all pair columns test was performed using GraphPad Prism version 5.0 software for windows (GraphPad Prism San Diego California USA). A p-value <0.01 was considered to be statistically significant, while those p-value<0.05was considered to be highly significant.

3. Results and discussion

Polymeric materials have proven as useful support systems to promote cellular growth in artificial tissue engineering. Their potential to mimic natural conditions has been observed to promote cell adhesion, proliferation, differentiation, ECM formation and ultimately tissue regeneration. Amongst the range of polymers that may be processed for scaffold fabrication, starch is a natural biopolymer that exhibits plentiful availability, complete biodegradation and hence safety, and potential for wound healing [9]. These properties, along with its economic nature, render it as a suitable material for fabricating an affordable scaffold product for extensive applications. The physicochemical properties (viscosity, permeability, water absorbency, gel formation) of starch make it amenable for processing by electrospinning [18,19], a method that can produce uniform and aligned nanofibers with dimensions similar to that of natural ECM. Furthermore, this process, which was originally used in textile industry, is suitable for scale-up allowing generation of commercial quantities of nanofibrous materials. However, processing of natural biopolymers, like starch, by electrospinning is a challenging task that was addressed in the scope of present research.

3.1. Preparation of nanofibers using electrospinning

Morphology of nanofibers is largely influenced by several factors including viscosity, concentration, conductivity and the surface tension of polymeric solutions that are processed. Starch to PVOH (S/PVOH) ratio was maintained at 30:70 w/w during the experiments as the ratios containing higher percentages of starch or equivalent weights of starch and PVOH did not yield fibers of sufficient mechanical strength (data not shown). Starch is hydrophilic and moisture sensitive polysaccharide that makes it difficult to be processed by electrospinning. Also starch undergoes gelatinization upon heating due its constituents, amylose and amylopectin. The solution crystallizes upon cooling, the phenomenon termed as retrogradation of starch [11]. Hence incorporation of a plasticizing agent like PVOH is highly critical for electrospinning starch nanofibers for improving the uniformity and the bonding between polymer chains in solution [12]. Furthermore, PVOH is a non-toxic, biocompatible semi-crystalline polymer, which possesses excellent strength, gas permeability and thermal characteristics [20]. Hence inclusion of higher amount of PVOH in the polymer blend was not anticipated to negatively influence the scaffold properties during cellular investigations.

3.2. Effect of polymer properties and solvent system on fiber formation

The concentration and hence viscosity of the polymeric solution bear the most significant influence on fiber properties. Further, the concentration of polymeric blend influences the properties of electrospun fibers. At low polymeric concentration, surface tension dominates viscoelastic forces and results in beaded and non-uniform fiber formation. Whereas, at high concentrations

viscosity increases which affects jet or Taylor cone formation and hence spinning, resulting in formation of thicker fibers [21]. The initial trials taken with aqueous polymer solutions lower than 10% w/v resulted in electrospraying. This was conjectured to be due to lower conductivity of polymer solution as stated in earlier reports, with alternate polymers [22]. In order to promote sufficient long-chain entanglement between polymer chains to enable formation of continuous fibers, the polymer blend was dissolved in a mixture of water and 10% v/v of ethanol, based on its ability to solubilize the polymers (data not shown) and to avoid the cellular toxicity associated with alternative organic solvents like dimethyl sulfoxide that have higher solubilization potential for starch [23,24]. Also inclusion of a non-hazardous solvent like ethanol was thought to be suitable to enable its easy removal from the fibers at a later stage.

3.3. Effect of flow rate

At the optimum flow rate the feeding rate is proportional to the electrospinning speed, which results in stable Taylor cone formation and formation of uniform fibers due to sufficient evaporation of residual solvent. A lower flow rate is desirable to produce fibers of smaller diameter as it enables solvent removal until the polymer-fluid jet reaches collector [25]. In our study, we found that the flow rate of 0.3 mL/h resulted in slightly reduced fiber diameter than that with 0.5 mL/h as stated in Table 1. At flow rates deviating from the optimum, asymmetric Taylor cones are formed which results in production of fibers with wide distribution. Although the fiber diameter with lower flow rate (0.3 mL/h) was slightly lesser than that obtained with a higher flow rate (0.5 mL/h), the mechanical strength of the former fibers was significantly lower than the fibers obtained with higher flow rates. Also at higher flow rates (>0.5 mL/h), more amount of polymer solution is ejected through the tip, which results in thicker fibers (results not shown as nanofibers were not obtained). Thus, for further studies the flow rate was optimized at 0.5mL/h.

3.4. Effect of tip to collector distance (TCD) and collector type

The TCD governs the average diameter of electrospun fibers by affecting the strength of electric field and hence their stretching. It has been reported that increased distance results higher jet instability, which increases the fiber diameter and number of beads [26]. The TCD has also been known to influence fiber morphology. At shorter TCDs, the electrical field is strong and produces whipping instability that may result in multiple jet formation and beaded fiber formation [16]. In case of very high distances, the strength of electric field becomes too weak to support adequate deposition of fibers over the collector. Thus the optimization of TCD becomes important factor to obtain uniform and bead free fibers. When the experiments were carried out at TCD of 23 cm, at the voltage of 25 kV, the resulting fibers possessed lower mechanical strength (<10 kPa). However, when the process was performed at 13 cm, at the voltage of 25 kV, the mechanical strength of the fibers improved to values between 10.32 and 16.58 kPa, with varying polymer concentrations, as shown in Table 3. The values further improved by crosslinking with glutaraldehyde, as discussed in the subsequent sections of this manuscript. Improved mechanical strength when spinning was done at lower TCD may be attributed to appropriate collection of fibers over the collector because of reduced TCD. Generally, while spinning the electric field is generated this is dependent of TCD and the voltage. This electric field determines rate of fiber formation. In our findings it was observed that the fibers collected at drum collector have uniformity in terms of mechanical value (data not shown) as compared to that of plate collector. Thus the drum type of collector was used for experiments.

Table 1
Influence of flow rate on fiber diameter.

Flow rate of polymer solution	Polymer concentration (% w/w)	Fiber diameter (nm)
0.3 ml/h	10	172.9 ± 17.83
	12	185.2 ± 7.96
	14	220.1 ± 29.37
0.5 ml/h	10	173.3 ± 19.14
	12	206.3 ± 13.28
	14	237.0 ± 22.52

3.5. Effect of voltage and polymer concentration

The electric field strength, which is the ratio of voltage to distance, also has a significant impact on the fiber diameter. Researchers observed that at lower starch concentrations, the voltage require to pull the jet was more compared to that required at high concentrations [27]. Furthermore, Sukigara et al. [28] have reported any deviation from optimum ratio of voltage to distance was found to increase the fiber diameter. It has further been reported that reduction in the electric field strength results in decreased electric stress on the starch dispersion, which results in reduced efficiency in jet formation. On the other hand increasing the electric field strength accelerates the jet with a very high speed to result in high instability and formation of beaded fibers. Although fiber formation occurs when the voltage reaches its threshold values, contradictory results have been reported regarding the effect of voltage during electrospinning. Reneker et al. [29] have reported no significant impact on fiber morphology due to applied voltage. While Zhang et al. [30] have stated that higher voltage results in ejection of more polymer, which leads to formation of thicker fibers [31], and beaded morphology [32,33]. Also higher voltage has been known to increase the electrostatic forces, resulting in increased split ability and rapid ejection fiber from the needle end [25].

In our study, three different voltages viz. 15 kV, 25 kV and 35 kV were employed to study their effect on fiber formation at 13 cm TCD. At 15 kV, fiber formation was not observed, probably due to generation of insufficient electric field. Figs. 1 and 2 represents the effect of voltage (35 and 25 kV) on size of nanofibers at various polymer concentrations. At 25 kV voltage, uniform and thin nanofibers (<160 nm) were observed, without any beads. Figs. 1D and 2D represents relationship of polymer concentration versus fiber diameter at 25 kV and 35 kV, respectively. A voltage of 35 kV resulted in thick, beaded fibers shown Fig. 2D. Thus, a voltage of 25 kV was considered to be suitable for fabrication of nanofibers, as shown in Fig. 1D. Further, the fiber morphology is influenced by the viscosity as well as surface tension of polymer solution. Surface tension tends to reduce surface area per unit mass that results in formation of droplets or particles while viscosity promotes fiber formation. At low polymeric concentration, surface tension dominates viscoelastic forces and results in formation of beaded and non-uniform fibers. On the contrary, higher concentrations result in viscous solutions that affect jet or Taylor cone formation and hence spinning, thus giving thick fibers. In this study, formation of uniform fibers was observed at higher polymer concentration of 14% w/v. Concentrations lower than 10% w/v resulted in electrospraying, rather than spinning.

3.6. Mechanical strength analysis

The tensile or mechanical strength of nanofibers plays an important role during their end-application. Salgado et al. [34] reported that the tensile strength measures the force required to

Table 2
Solution process parameters optimized for electrospinning of nanofibrous mats.

Solution Parameters	
Polymer concentrations	10, 12, 14 %w/v
Starch: PVOH	30:70 w/w
Solvent System	10% Ethanol
Electrospinning process Parameters	
Applied voltage	25 kV
Spinning Distance	13 cm
Flow rate	0.5 ml/h

Table 3
Effect of tip to collector distance (TCD) on mechanical strength and diameter of nanofibers.

Tip to collector distance (cm)	Conc.(% w/v)	Mechanical Strength (kPa)	Diameter (nm)
23	10	6.2	144.7 ± 10.13
	12	7.8	168.9 ± 27.08
	14	9.6	269.0 ± 23.89
13	10	10.32	94.18 ± 3.61
	12	12.70	118.8 ± 11.84
	14	16.58	162.1 ± 27.02

withstand the maximum stress per unit area for a sample. The nanofibrous mats were analyzed for mechanical strength by universal tensile machine. The mechanical strength of a single layer of S/PVOH nanofibrous mat was found in range of 10–15 kPa, which is sufficient to maintain structural integrity during the *in vitro* and/or *in vivo* growth and remodeling process. The achieved mechanical properties are in accordance with previous reports [34]. However, the resulting nanofibrous mats easily dissolved in water in less than 0.5 h due to hydrophilic nature of starch and the PVOH. Therefore, these nanofibrous mats were further cross-linked to improve their mechanical strength and wet-stability to values sufficient for promoting cell growth and proliferation. Various cross-linkers have been reported including polyamide epichlorohydrin resin, glyoxylated polyacrylamide resin, formaldehyde derivatives and glyoxal [23]. Among these, glutaraldehyde is frequently used for tissue engineering applications. In this study, various concentrations of glutaraldehyde were studied for their cross-linking ability and optimized depending upon the enhancement in water stability. When the mats cross-linked using higher concentrations of glutaraldehyde (25 and 15% v/v) were incubated with cell culture medium to be used in subsequent cellular studies, the medium turned highly acidic as indicated by its pale yellow color, which may be due to incomplete removal of glutaraldehyde or glycine. Thus these were considered unsuitable for further studies, as they would result in cellular toxicity. When cross-linking was conducted with lower concentrations i.e. at 5%v/v glutaraldehyde, the resulting products dissolved within 4 h in water, which indicated insufficient mechanical strength due to lower degree of cross-linking. Thus optimum crosslinking was observed at a concentration of 12.5%v/v of glutaraldehyde. The tensile strength of crosslinked nanofibers(CNF) mats increased to 0.57 MPa, 0.79 MPa and 0.88 MPa, respectively for mats containing 10, 12 and 14% w/v of polymer blend, which was within the acceptable limits as reported in literature [35]. Several studies have reported varying values of tensile strength ranging from 0.7 to 18.0 MPa as sufficient for dermal cell culture [36–38]. Also, the nanofibrous scaffolds can have the potential as wound dressing bandage or film that may be applied to the skin to allow cell regeneration by mimicking natural ECM. Further, our CNF mats were found to be stable over a period of 28 days. ATR-FTIR analysis was conducted to check presence of traces of glutaraldehyde or glycine, which showed no chemical change due to glutaraldehyde or glycine. Thus, these cross-linked nanofibers were used for further cellular studies. Table 2 depicts the optimized parameters for polymer solution and electrospinning process that was employed to process nanofibrous mats for further studies.

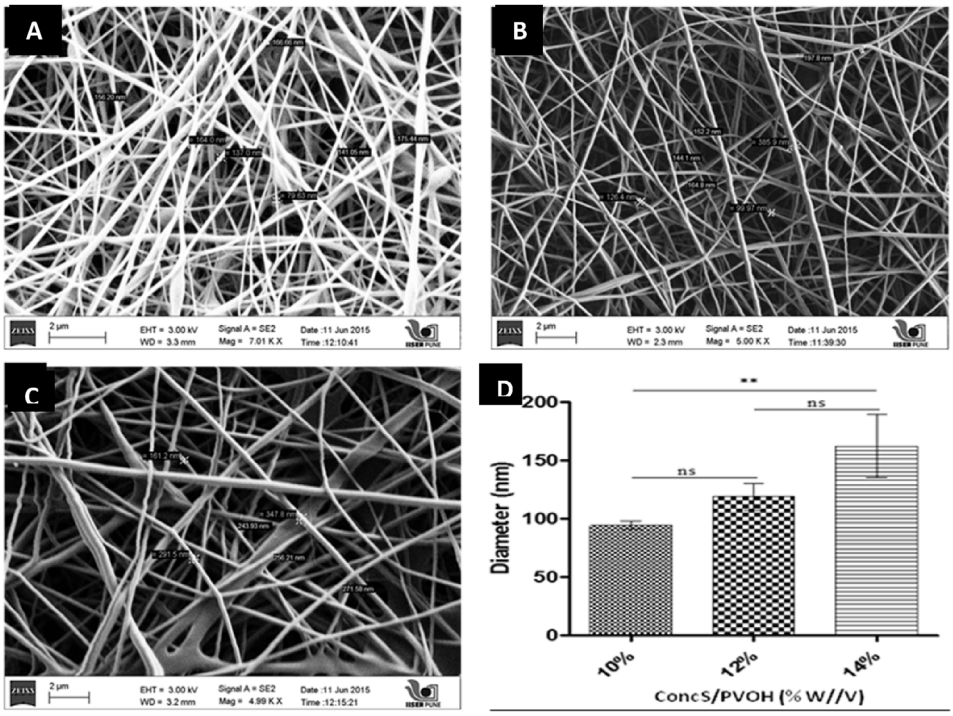

Fig. 1. SEM images of nanofibers at polymer concentrations of (A) 10%w/v, (B) 12%w/v and (C) 14%w/v at polymer ratio 30:70%w/w of S/PVOH with 0.5 mL/h flow rate and (D) graph relationship of S/PVOH concentration versus diameter at 25 kV Voltage [*p-value <0.05, **p-value <0.01, ns: non-significant (p-value >0.05)].

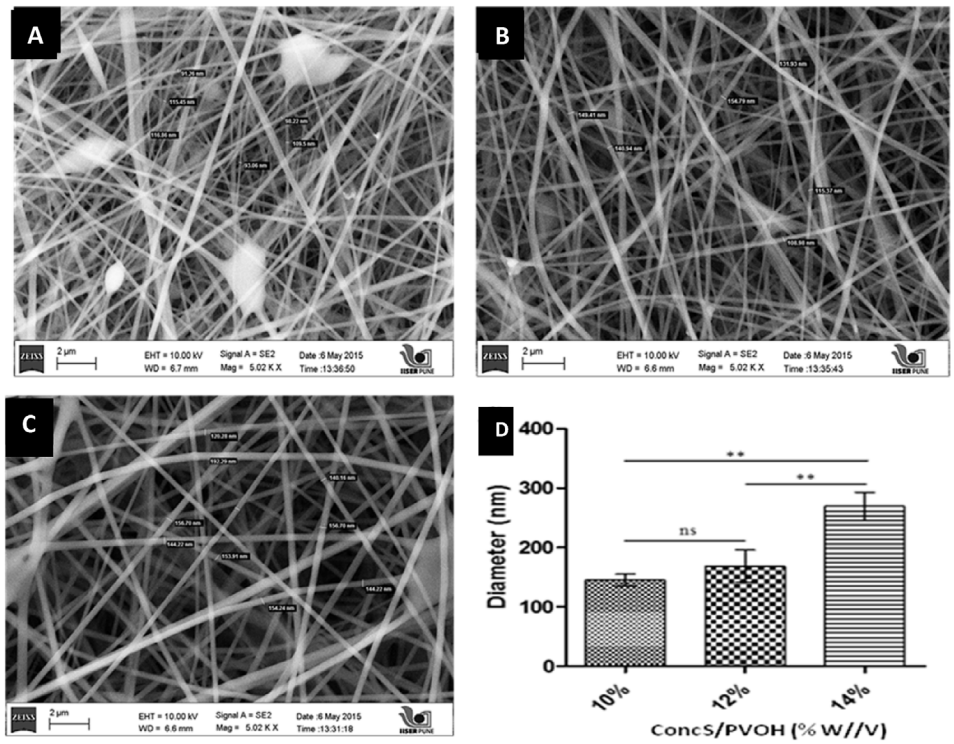

Fig. 2. SEM images of nanofibers at polymer concentrations of (A) 10%w/v, (B) 12%w/v and (C) 14%w/v at polymer ratio 30:70%w/w of S/PVOH with 0.5 mL/h flow rate and (D) graph relationship of S/PVOH concentration versus diameter at 35 kV Voltage [*p-value <0.05, **p-value <0.01, ns: non-significant (p-value >0.05)].

3.7. *Attenuated total reflectance-fourier transform infrared spectroscopy (ATR-FTIR)*

Molecular and the functional group characterization were carried out using ATR-FTIR to understand the polymer interaction and confirm any unfavorable interaction. The spectra of starch and PVOH were taken as control and compared with that of the mats (Fig. 3). In case of spectrum of starch, characteristic peak at 3300-3400 cm^{-1} confirmed the presence of OH and COOH groups. The broad band at 2900 and 3000 cm^{-1} were indicative of -CH_2 and -CH_3groups, respectively [38]. The presence of -OH stretching vibrations at 3292 cm^{-1} and the -CH stretch of alkane could be seen at 2918 cm^{-1} in IR graph of starch. The sharp peak at 992 cm^{-1} was attributed to =C-H bend [39].

Similarly in case of PVOH, the dominant absorption peaks at 3306 cm^{-1}, 2926 cm^{-1}, 1712 cm^{-1} and 1129 cm^{-1} were attributed to the -OH stretch of carboxylic acids, CH-OH, C=O, C-O of pure PVOH, respectively [36]. The band at 1329 cm^{-1} was observed due to coupling of OH in plane vibrations and the band at 1424 cm^{-1} was CH wagging vibrations [34]. The spectra of nanofibrous mat containing 10%, 12% and 14% w/v of polymer blend exhibited presence of both the polymers. Here, −OH stretch was observed between 3100 and 3400 cm^{-1}, which indicated the presence hydroxyl groups of both starch and PVOH. The characteristic -CH stretching vibrations were observed at 2800 to 2900 cm^{-1}. The sharp peaks at 1727 cm^{-1} and 1724 cm^{-1} confirmed the presence of −C=O bonding of carboxylic acid functional group of starch. Peaks were observed at 1080 cm^{-1} to 1150 cm^{-1} showing C-O-H groups of alcohol and carboxylic acid. The characteristic bands at 1000 to 1300 cm^{-1} corresponded to the C-O stretch of alcohols and carboxylic acids [40]. The region between 1100 and 1200 cm^{-1} and the peak at 1129 cm^{-1}, were contributed by the crystallinity of PVOH [32]. The peak at 1022 cm^{-1} observed in the spectra of nanofibrous mats was due to the amorphous nature of starch that was contributed by its heating at 70 °C, during the preparation of starch solution [17]. There was no significant peak shift observed in any of the IR spectra of nanofibrous mats, which indicated absence of any chemical interaction during electrospinning. In Fig. 4, crosslinked scaffolds exhibited the peak at around 2925 cm^{-1}, corresponding to C-H stretching of aldehyde group of glutaraldehyde. These results, which are consistent with earlier reports [41,42], which confirmed the crosslinking of nanofibers with glutaraldehyde. Thus, the study revealed absence of any unfavorable chemical interaction between the polymers leading to altered properties of nanofibers. Thus fiber formation was successful at 30:70 w/w ratios of starch and PVOH, at

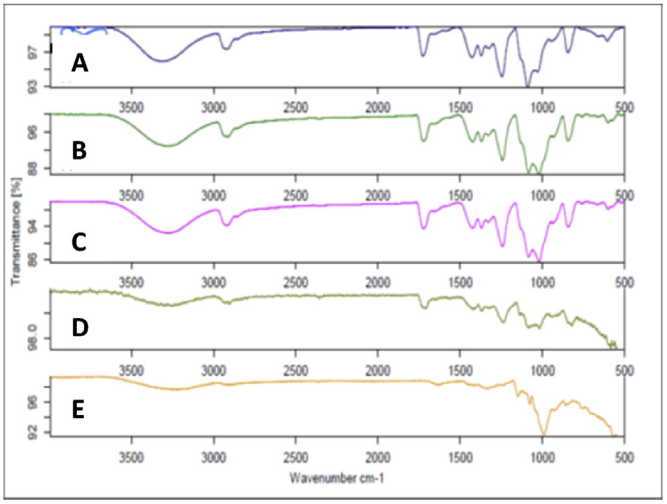

Fig. 3. ATR-FTIR spectra (A) pure starch, (B) pure PVOH, (C) 10%w/w, (D) 12%w/w, (E) 14%w/w S/PVOH nanofibers.

the voltage of 25 kV. No peak indicative of amine or aldehyde was observed, which suggested that the CNF had no traces of glutaraldehyde or amine and hence can be considered for cellular investigations.

3.8. Differential Scanning Calorimetry

DSC of individual polymers as well as the nanofibrous mats was recorded to analyze the variations in thermal transitions that may have occurred during the process of electrospinning. During this process, we expect phase transition of polymer and rapid solvent evaporation [43]. In-process electrospinning measurements, we also expect that high elongation of the polymeric network results in stretching of polymer macromolecules and consequently in the formation of nanofibers with a high degree of molecular orientation [44]. Thermal transitions occur when pure starch is heated with aqueous media, which is called as gelatinization of starch. The process can be defined as the one in which insoluble starch are converted into a solution of its constituent molecules [45]. In our investigation, *Tg* (glass transition temperature) of starch was observed at the temperature of 88.49 °C (Fig. 5A), which was higher than the reported values. Generally, the first endothermic or 'G curve' is indicative of the glass transition temperature of a polymer, which for starch is known to range between 61 and 85 °C [46]. The increase in glass transition temperature may be attributed to variation in amylose content of our starch sample as compared the ones reported in literature. The increase in onset temperature may have been because of the heat supplied to the solution that may have lead to the disruption of hydrogen bonds between the branched chains of amylose and amylopectin [17]. Moreover researchers have reported that although the DSC curves of polysaccharides do not exhibit any clear *Tg* features, crystalline regions exists in some crystalline polysaccharides due to presence of strong intra- and inter-hydrogen bonding and heterocyclic units [47]. When the crystallites are more stable, they need excess thermal energy to breakdown the structures, which results in a second endothermic called 'M1 curve.' In our study, this was observed in case of PVOH, as shown in Fig. 5B, the curve at 323.08 °C was thought to be due to excess thermal power required to degrade the crystallites. The *Tg* of PVOH was observed at 76.74 °C, whereas the melting point was seen at 195.5 °C. The melting point of the PVOH is dependent on its molecular weights. While the melting of crystallites is controlled by its molecular mobility in amorphous region [47]. The DSC thermo grams of nanofibrous mats formulated with 10, 12 and 14% w/v of polymer blend have been depicted in Fig. 5C, D and E. The studies revealed that as the concentration of polymeric solution was increased from 10% w/v to 12%w/v and then 14%w/v, there was an increase in the glass transition temperatures of the fibrous mat from 71.81 °C to 72.92°Cand then 75.26 °C. However, the *Tg* in case of all nanofibers was lower than that of the individual polymers. This decrease may be due to high mobility of molecules and formation of strong intermolecular hydrogen bonds within the polymers during fiber formation [48,49]. In other words, this may also due to improved orientation of molecular chains, lower entanglement of polymers and higher surface area to volume ratio of the electrospun nanofibers. Similar observations have been reported by other researchers for PLGA nanofibers prepared by electrospinning [50]. Further, the crystallinity of nanofibers decreased sharply after crosslinking with glutaraldehyde. Glutaraldehyde forms covalent bridges between polymers chains and may act as a separator between the individual chains, thereby causing a reduction in the crystallinity. This observation is similar to the results obtained by researchers with polyvinyl alcohol nanofibers used in fuel cell applications [51].

3.9. Thermogravimetric analysis (TGA)

Generally, in wound healing, a period of one month is required to regenerate the cells and formation of new tissues [52–54]. Thus, to get newly formed tissues, the nanofibers should not degrade for at least 29 days. Since the end-application of our nanofibrous mats would be in wound healing, the nanofibers were treated with medium having pH similar to that of body fluid. The mats were incubated at 37 °C in phosphate buffer saline pH 7.4 and loss in their mass was analyzed on 0, 7, 14, 28 days by TGA for. It was observed that for pure starch and PVOH powder, as well as the nanofibrous mats, the degradation took place in two distinct steps. The thermograms exhibited two distinct regions of weight losses, the first one region corresponding to the loss of moisture retained by the polymers and the nanofibrous mats. As seen from Fig. 6A, the weight loss in case of pure starch powder was found to be more pronounced in the first step when compared with that of pure PVOH, as starch absorbs more moisture due to the presence of carboxyl groups [55]. It was found that a weight loss of 17% occurred in case of starch 100 °C, while for PVOH it was not more than 5%. Also the degradation profile of starch exhibited 20% weight loss at 278 °C, which may be attributed to the degradation of amylose present in the starch [56]. Further, the degradation profile displayed a significant weight loss of 65% was observed at 313 °C, which may be depictive of pyrolysis of starch [46].

The degradation profile of pure PVOH powder has been represented in Fig. 6B. Once again, the profile revealed evaporation of moisture, along with some volatile residues such as alcohol. TGA graph of PVOH (Fig. 6B) showed that the first step of degradation was quite narrow. Further, PVOH showed lower weight loss of 7.8% near its melting temperature i.e. 230 °C. There was no significant weight loss observed when compared with starch. The initial decomposition was mainly due to dehydration of hydroxyl groups as also reported elsewhere [57].

In case of cross-linked scaffolds(Fig. 6C, D, E), the presence of a small peak at around 215 °C was thought to be due to the breakage of cross-linkages during first stage of degradation. Also varied end set temperature was observed, which indicated that there may be generation of various inter-component bonds in presence of cross-linker, which may have given rise to different three-dimensional networks and a complex degradation behavior. Similar observations have been reported earlier in case of alternative cross-linked scaffolds [58]. On day 14, the weight losses found were 76%, 68% and 77% for the mats containing 10%, 12% and 14% w/v of polymeric blends at 481 °C, 451 °C and 485 °C, respectively. On day 28, it was found that the weight loss for the mat containing 10% w/v of polymeric blend was 81% at 478 °C, while for the mat containing 12% w/v of polymeric blend it was 77% at 444 °C, and for the mat containing 14% w/v of polymeric blend, it was 72% at 471 °C (Fig. 6E). The difference in % weight loss is very low between 14 days and 28 days. From 14 days to 28 days, the % of weight loss is increased to 5% and 9% with 10% and 12% of S/PVOH, respectively. The % weight loss decreased to 5%, with 14% S/PVOH, after 28 days compared to 14 days. It was observed that the curve elongated until threshold temperature of the instrument. Small amount of residue (23%) was observed at this temperature, suggesting that degradation of CNF mats would occur at a temperature of more than 500 °C and that cross-linked mats can sustain more temperature. From the analysis, it was interpreted that the nanofibrous scaffolds containing 10% w/v of polymer blend degraded almost completely at the end of study, leaving behind a residue of only ~5%. However, the mats containing 12% and 14% w/v of polymeric blend did not completely degrade at maximum temperature limit of the instrument and would require a higher temperature for degradation. Thus, the scaffolds containing higher polymer concentrations may

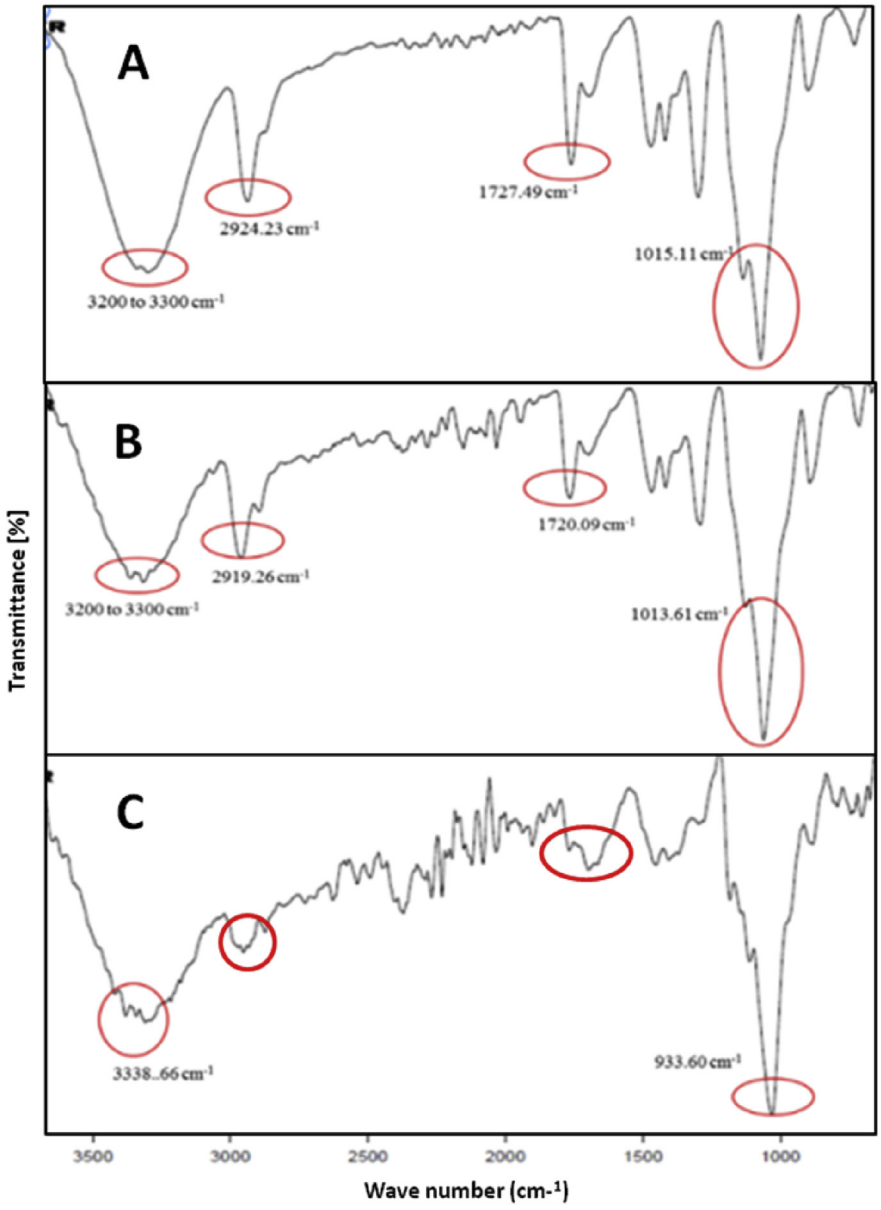

Fig. 4. ATR-FTIR spectra of cross-linked nanofibrous mats fabricated using 30:70%w/w of (A) 10%w/v, (B) 12%w/v, (C) 14%w/v of S/PVOH.

be useful for wound healing applications since they are likely to permit proliferation of cells and allow tissue regeneration during the time required for healing.

3.10. Water uptake

The water uptake and the absorption capacity are the most important properties for polysaccharides, especially for biodegradable polymers. As reported in earlier studies, cells need moist environment to survive and proliferate [59]. One of the major drawbacks of using starch is its water absorption tendency. Starch is water sensitive and PVOH is a hydrophilic polymer, which resulted in a water sensitive blend. A decrease in water sensitivity for the nanofibrous film is very important for biomedical application [60]. Between both the polymers, PVOH has been reported to result in a much lower water uptake than starch [61]. In our work, the water absorption capacity of cross-linked scaffolds was studied for 15 days. The samples were weighed at specific time intervals and the percent weight losses were calculated. It was found that the water retention property of the nanofibers increased for 3 days and then sharply decreased. The reduction in water absorption of nanofibers was found after 5 days. Fig. 7 represents water uptake property of nanofibrous mats containing 10%, 12% and 14%w/v of 30:70%w/w of starch and PVOH at day 1, 2, 5 and 7. After 7 days, further reduction in water uptake was not observed. The decrease in water uptake may due to shrinkage of nanofibers and due to loss in their porous structure in water, which resists the uptake of water into the nanofibers. Several other authors have also reported similar results. Chen et al. [20]have proposed that the declining water uptake may be due to tight hydrogen bonding and the shielding effect of hydroxyl and the carboxylic groups present in the polymers, probably due crosslinking of nanofibers with glutaraldehyde.

3.11. Cellular proliferation and cytotoxicity

The cell viability of the crosslinked nanofiber mats (CNF) was

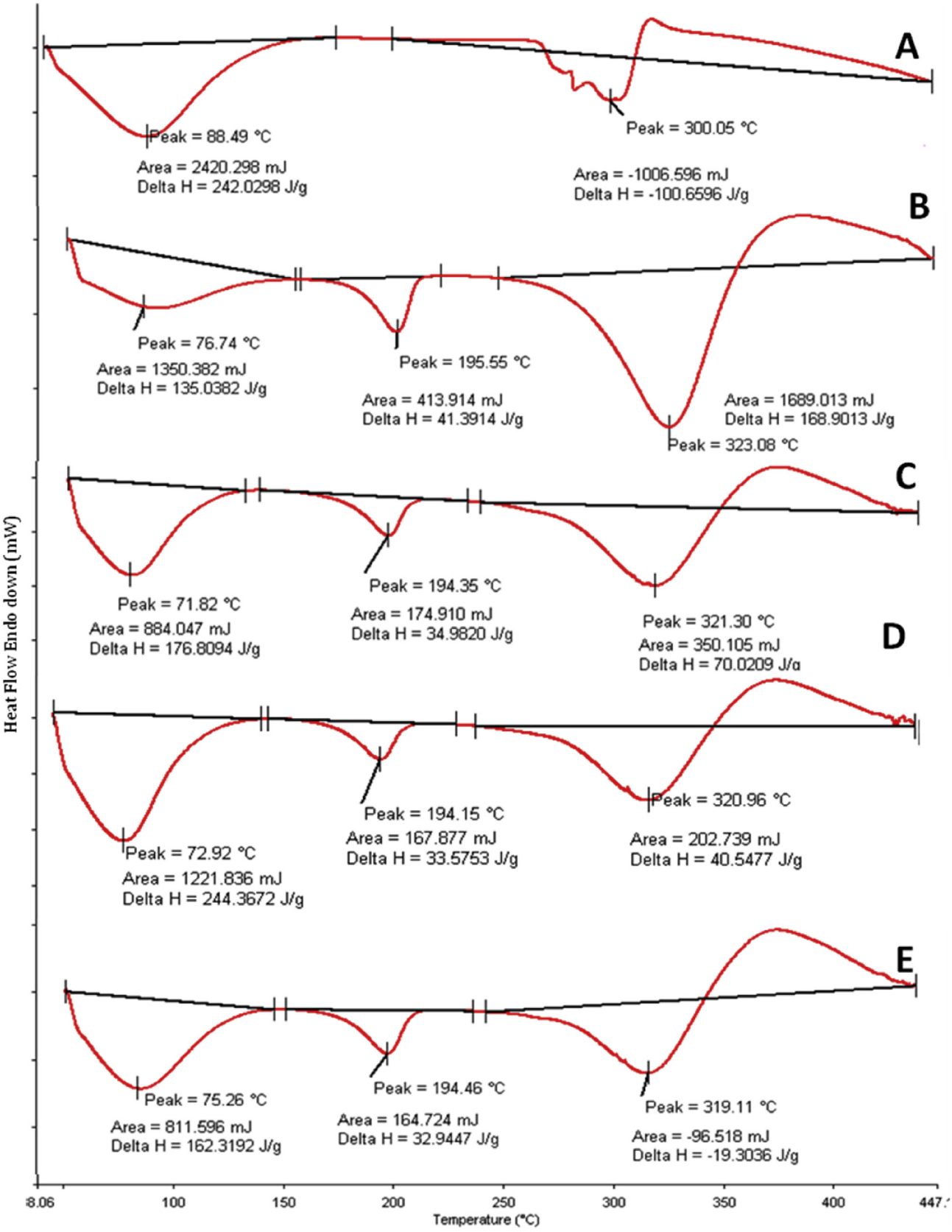

Fig. 5. DSC thermograms of (A) Starch and (B) PVOH; nanofibrous mat fabricated using (C) 10%w/v, (D) 12%w/v, (E) 14% w/v of 30:70 w/w S/PVOH at 25 kV.

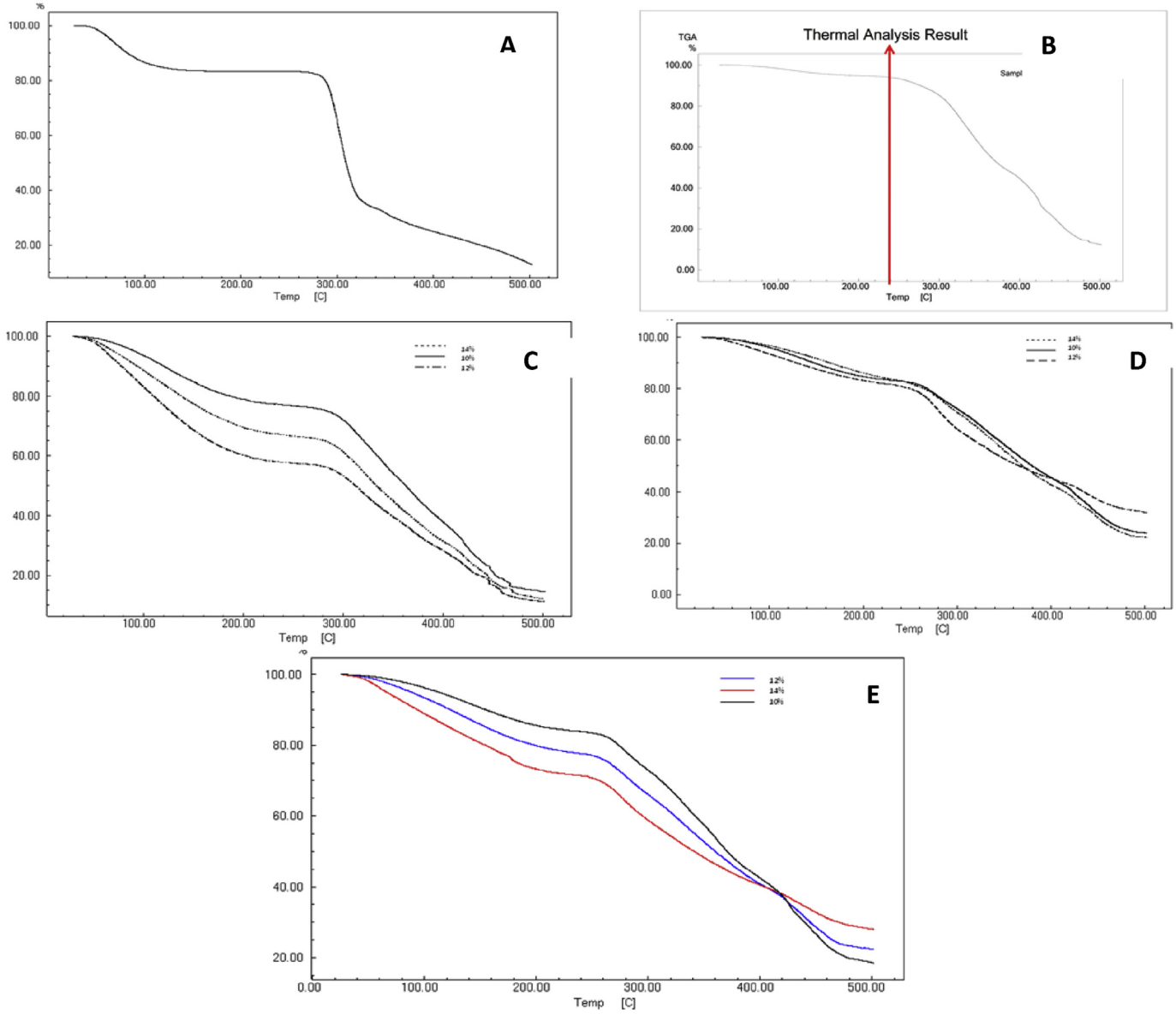

Fig. 6. TGA profiles of the (A) pure starch and (B) PVOH; CNF mat (C) at day 0, (D) at day 14 and (E) at day 28 containing S/PVOH at 10%w/w, 12%w/w and 14%w/w.

assessed using EZBlue dye assay. The growth of mouse fibroblast cells was studied on days 1, 3, 5 and 7. In general, the cell growth can be observed in four stages, a) protein adsorption at the surface, b) contact of rounded cells, c) attachment of cells to substrate and d) spreading of cells [62]. Moreover, Gundle et al. [63]have stated that the initial cell attachment usually occurs within four hours of after cell seeding; however this time may vary depending upon the type of cells used and the nature of substrate. During the assay, scaffolds in medium were used as control. The cells started to span across the scaffolds due to pores present on nanofibrous mats, which acted as a template and support. At day 3, cells almost completely filled the pores present on all the scaffolds. No significant change in cell viability was observed on the scaffolds. Fig. 8 demonstrates growth of mouse fibroblasts on the nanofibrous scaffolds at day 5. Linear cell proliferation was seen on scaffolds containing 10% w/v of S/PVOH. However, the rate of cell proliferation was reduced in case of scaffolds containing 12% and 14% w/v of S/PVOH after day 5 of culture. The low cell growth may due to the variations in the scaffolds surface area upon absorption of cell

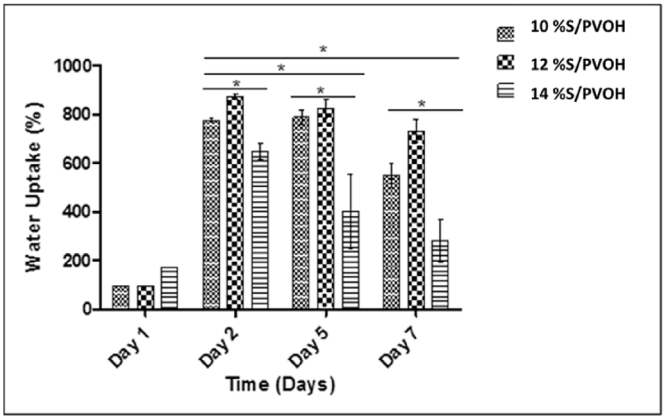

Fig. 7. Water uptake property of nanofibrous mats containing 10%, 12% and 14%w/v of 30:70%w/w of starch and PVOH.

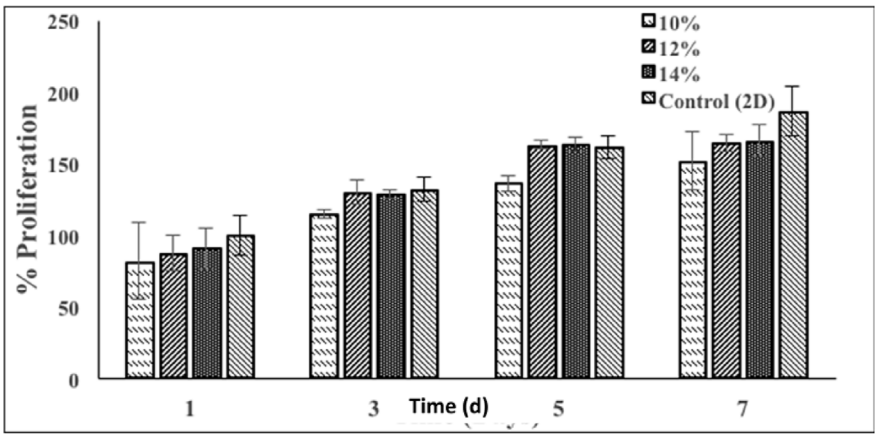

Fig. 8. Cell proliferation activity of mouse fibroblasts cells cultured on respective scaffolds for 1, 3, 5, and 7 days in culture ($n = 3$).

culture medium. This may have resulted in non-homogeneous cell growth throughout the entire scaffold and concentrated growth only in some areas [34]. In our investigation, only 80% cell proliferation was observed in case of all the nanofibrous mats. It was observed that the cells exhibited a greater tendency to spread or proliferate for scaffolds containing low polymeric concentration i.e. for 10% w/v of S/PVOH. While in case of the scaffolds containing higher polymeric concentrations i.e. 12% w/v of and 14% w/v of S/PVOH, the values of optical density remained similar for day 5 and day 7 as shown in Fig. 8. This indicated that the cells may have reached confluence.

However, cell growth was observed in all the scaffolds, indicating their biocompatibility. Cell growth is accumulation of mass or cells which occurs at specific time and places which may be dependent on nutrients or growth factors [64]. In this investigation, although the nanofibrous mats were non-toxic to the cells, we contemplate that addition of growth factors or the nutrients may enhance the cell growth and proliferation, which is being conducted. Overall results indicate that the developed scaffolds are able to support the growth and colonization of mouse fibroblasts. Although the developed nanomaterials has potential of scaffold for biomedical applications like wound healing, further investigations are in progress towards deeper understanding of their influence on cell growth.

4. Conclusions

Electrospun, starch-based nanofibrous mats were successfully fabricated using 30:70%w/w of starch and PVOH, at a voltage of 25 kV, flow rate of 0.5 mL/h and a TCD of 13 cm. This ratio of polymers yielded fibers with dimensions suitable for wound healing applications. Higher starch percentages lead to thicker fibers. Further, the average fiber diameter was also observed to be a function of polymer concentration and increased at higher polymer concentrations. A long spinning distance was found to generate a weak electric field and hence hampered fiber formation. Electrospinning at lower voltage did not result in nanofiber production, while a higher voltage resulted in increased fiber diameter, without affecting their mechanical properties. Cross-linking improved the mechanical and thermal properties of the fabricated nanofibrous scaffolds. This may be due to interaction between aldehyde group of glutaraldehyde and polar hydroxyl groups present in starch and PVOH. Cellular investigations revealed that the nanofibrous mats allowed cell growth and proliferation of dermal cells and have a potential to be employed in biomedical applications like wound healing. Outcomes from elaborate cellular investigations and animal studies, coupled with the low cost of raw materials and the process, can make the final product an economical solution for wound healing management amongst patients belonging to lower socio-economic strata of society.

Conflict of interest

The authors declare no conflict of interest.

Acknowledgements

Ms. Vijaya Waghmare is thankful to Technical Education Quality Improvement Program (TEQIP), Government of India for research fellowship. The authors wish to thank Ramanujan Fellowship Grant (SR/S2/RJN-139/2011), Department of Science and Technology, Government of India; Ramalingaswami Fellowship Grant (BT/RLF/Re-entry/51/2011), Department of Biotechnology, Government of India; and Rajiv Gandhi Science and Technology Commission (RGSTC/File-2013/DPP-108/CR-19), Government of Maharashtra, for funding.

References

[1] F. Rosso, G. Marino, A. Giordano, M. Barbarisi, D. Parmeggiani, A. Barbarisi, Smart materials as scaffolds for tissue engineering, J. Cell. Physiol. 203 (2005) 465–470.
[2] X. Xin, M. Hussain, J.J. Mao, Continuing differentiation of human mesenchymal stem cells and induced chondrogenic and osteogenic lineages in electrospun PLGA nanofiber scaffold, Biomaterials 28 (2007) 316–325.
[3] J.M. Holzwarth, P.X. Ma, Biomimetic nanofibrous scaffolds for bone tissue engineering, Biomaterials 32 (2011) 9622–9629.
[4] S. Pérez, E. Bertoft, The molecular structures of starch components and their contribution to the architecture of starch granules: a comprehensive review, Starch Stärke 62 (2010) 389–420.
[5] A. Salgado, O. Coutinho, R. Reis, Novel starch-based scaffolds for bone tissue engineering: cytotoxicity, cell culture, and protein expression, Tissue Eng. 10 (2004) 465–474.
[6] S. Baghaie, M.T. Khorasani, A. Zarrabi, J. Moshtaghian, Wound healing properties of PVA/starch/chitosan hydrogel membranes with nano Zinc oxide as antibacterial wound dressing material, J. Biomater. Sci. Polym. Ed. (2017) 1–40.
[7] A. Hassan, M.B.K. Niazi, A. Hussain, S. Farrukh, T. Ahmad, Development of antibacterial PVA/starch based hydrogel membrane for wound dressing, J. Polym. Environ. (2017) 1–9.
[8] B. Amal, B. Veena, V. Jayachandran, J. Shilpa, Preparation and characterisation of Punica granatum pericarp aqueous extract loaded chitosan-collagen-starch membrane: role in wound healing process, J. Mater. Sci. Mater. Med. 26 (2015) 181.
[9] B. Amal, B. Veena, V. Jayachandran, J. Shilpa, Preparation and characterisation of Punica granatum pericarp aqueous extract loaded chitosan-collagen-starch membrane: role in wound healing process, J. Mater. Sci. Mater. Med. 26 (2015)

1–9.
[10] C.R. Weinstein-Oppenheimer, A.R. Aceituno, D.I. Brown, C. Acevedo, R. Ceriani, M.A. Fuentes, F. Albornoz, C.F. Henríquez-Roldán, P. Morales, C. Maclean, Research the effect of an autologous cellular gel-matrix integrated implant system on wound healing, Cell 151 (2010) 16.
[11] J.D. Schiffman, C.L. Schauer, A review: electrospinning of biopolymer nanofibers and their applications, Polym. Rev. 48 (2008) 317–352.
[12] C.A. Bonino, M.D. Krebs, C.D. Saquing, S.I. Jeong, K.L. Shearer, E. Alsberg, S.A. Khan, Electrospinning alginate-based nanofibers: from blends to crosslinked low molecular weight alginate-only systems, Carbohydr. Polym. 85 (2011) 111–119.
[13] H. Fredriksson, J. Silverio, R. Andersson, A.-C. Eliasson, P. Åman, The influence of amylose and amylopectin characteristics on gelatinization and retrogradation properties of different starches, Carbohydr. Polym. 35 (1998) 119–134.
[14] P. Wadke, R. Chhabra, R. Jain, P. Dandekar, Silver-embedded starch-based nanofibrous mats for soft tissue engineering, Surf. Interfaces 8 (2017) 137–146.
[15] A. Califano, M. Anon, Differential scanning calorimetry of mung bean starch, J. Food Sci. 55 (1990) 771–773.
[16] C.M. Tierney, M.G. Haugh, J. Liedl, F. Mulcahy, B. Hayes, F.J. O'Brien, The effects of collagen concentration and crosslink density on the biological, structural and mechanical properties of collagen-GAG scaffolds for bone tissue engineering, J. Mech. Behav. Biomed. Mater. 2 (2009) 202–209.
[17] P.S. Kumar, S. Abhilash, K. Manzoor, S. Nair, H. Tamura, R. Jayakumar, Preparation and characterization of novel β-chitin/nanosilver composite scaffolds for wound dressing applications, Carbohydr. Polym. 80 (2010) 761–767.
[18] M. Valizadeh, S.A.H. Ravandi, S. Ramakrishna, Recent advances in electrospinning of some selected biopolymers, J. Text. Polym. 1 (2013) 70–84.
[19] G. Liu, Z. Gu, Y. Hong, L. Cheng, C. Li, Electrospun starch nanofibers: recent advances, challenges, and strategies for potential pharmaceutical applications, J. Control. Release 252 (2017) 95–107.
[20] Z. Chen, L. Zhang, L. Wang, Study on filming of oxidized starch/PVA, Front. Agric. China 5 (2011) 649–654.
[21] B. Subia, J. Kundu, S. Kundu, Biomaterial Scaffold Fabrication Techniques for Potential Tissue Engineering Applications, INTECH Open Access Publisher, 2010.
[22] J. Zeleny, Instability of electrified liquid surfaces, Phys. Rev. 10 (1917) 1.
[23] L. Kong, G.R. Ziegler, Fabrication of pure starch fibers by electrospinning, Food Hydrocoll. 36 (2014) 20–25.
[24] L. Kong, G.R. Ziegler, Role of molecular entanglements in starch fiber formation by electrospinning, Biomacromolecules 13 (2012) 2247–2253.
[25] J.S. Lee, K.H. Choi, H.D. Ghim, S.S. Kim, D.H. Chun, H.Y. Kim, W.S. Lyoo, Role of molecular weight of atactic poly (vinyl alcohol)(PVA) in the structure and properties of PVA nanofabric prepared by electrospinning, J. Appl. Polym. Sci. 93 (2004) 1638–1646.
[26] R. Milašius, Investigation of the possibility of forming nanofibres with potato starch, Fibres Text. East. Eur. 18 (2010) 82.
[27] L. Kong, G.R. Ziegler, Quantitative relationship between electrospinning parameters and starch fiber diameter, Carbohydr. Polym. 92 (2013) 1416–1422.
[28] S. Sukigara, M. Gandhi, J. Ayutsede, M. Micklus, F. Ko, Regeneration of Bombyx mori silk by electrospinning. Part 2. Process optimization and empirical modeling using response surface methodology, Polymer 45 (2004) 3701–3708.
[29] D.H. Reneker, I. Chun, Nanometre diameter fibres of polymer, produced by electrospinning, Nanotechnology 7 (1996) 216.
[30] C. Zhang, X. Yuan, L. Wu, Y. Han, J. Sheng, Study on morphology of electrospun poly (vinyl alcohol) mats, Eur. Polym. J. 41 (2005) 423–432.
[31] G.R. Ziegler, J.A. Creek, J. Runt, Spherulitic crystallization in starch as a model for starch granule initiation, Biomacromolecules 6 (2005) 1547–1554.
[32] O. Tretinnikov, S. Zagorskaya, Determination of the degree of crystallinity of poly (vinyl alcohol) by FTIR spectroscopy, J. Appl. Spectrosc. 79 (2012) 521–526.
[33] S. Yang, K.-F. Leong, Z. Du, C.-K. Chua, The design of scaffolds for use in tissue engineering. Part II. Rapid prototyping techniques, Tissue Eng. 8 (2002) 1–11.
[34] A. Salgado, M.E. Gomes, A. Chou, O. Coutinho, R. Reis, D. Hutmacher, Preliminary study on the adhesion and proliferation of human osteoblasts on starch-based scaffolds, Mater. Sci. Eng. C 20 (2002) 27–33.
[35] M. Kim, G. Kim, Electrospun PCL/phlorotannin nanofibres for tissue engineering: physical properties and cellular activities, Carbohydr. Polym. 90 (2012) 592–601.
[36] C.P. Barnes, S.A. Sell, E.D. Boland, D.G. Simpson, G.L. Bowlin, Nanofiber technology: designing the next generation of tissue engineering scaffolds, Adv. Drug Deliv. Rev. 59 (2007) 1413–1433.
[37] M.P. Prabhakaran, J. Venugopal, L. Ghasemi-Mobarakeh, D. Kai, G. Jin, S. Ramakrishna, Stem Cells and Nanostructures for Advanced Tissue Regeneration, Biomedical Applications of Polymeric Nanofibers, Springer, 2012, pp. 21–62.
[38] N. Nseir, O. Regev, T. Kaully, J. Blumenthal, S. Levenberg, E. Zussman, Biodegradable scaffold fabricated of electrospun albumin fibers: mechanical and biological characterization, Tissue Eng. Part C Methods 19 (2013) 257–264.
[39] C. Santos, C.J. Silva, Z. Büttel, R. Guimarães, S.B. Pereira, P. Tamagnini, A. Zille, Preparation and characterization of polysaccharides/PVA blend nanofibrous membranes by electrospinning method, Carbohydr. Polym. 99 (2014) 584–592.
[40] J. O'Brien, I. Wilson, T. Orton, F. Pognan, Investigation of the Alamar Blue (resazurin) fluorescent dye for the assessment of mammalian cell cytotoxicity, Eur. J. Biochem. 267 (2000) 5421–5426.
[41] N. Tudorachi, C. Cascaval, M. Rusu, M. Pruteanu, Testing of polyvinyl alcohol and starch mixtures as biodegradable polymeric materials, Polym. Test. 19 (2000) 785–799.
[42] B. Priya, V.K. Gupta, D. Pathania, A.S. Singha, Synthesis, characterization and antibacterial activity of biodegradable starch/PVA composite films reinforced with cellulosic fibre, Carbohydr. Polym. 109 (2014) 171–179.
[43] A. Arinstein, E. Zussman, Electrospun polymer nanofibers: mechanical and thermodynamic perspectives, J. Polym. Sci. Part B Polym. Phys. 49 (2011) 691–707.
[44] Z. Zhong, M.C. Wingert, J. Strzalka, H.-H. Wang, T. Sun, J. Wang, R. Chen, Z. Jiang, Structure-induced enhancement of thermal conductivities in electrospun polymer nanofibers, Nanoscale 6 (2014) 8283–8291.
[45] L. Kong, G.R. Ziegler, Formation of starch-guest inclusion complexes in electrospun starch fibers, Food Hydrocoll. 38 (2014) 211–219.
[46] J.W. Donovan, Phase transitions of the starch–water system, Biopolymers 18 (1979) 263–275.
[47] S.J. Lee, S.S. Kim, Y.M. Lee, Interpenetrating polymer network hydrogels based on poly (ethylene glycol) macromer and chitosan, Carbohydr. Polym. 41 (2000) 197–205.
[48] C.B. Roth, J.R. Dutcher, Glass transition and chain mobility in thin polymer films, J. Electroanal. Chem. 584 (2005) 13–22.
[49] L.M. Guerrini, M.P. de Oliveira, M.C. Branciforti, T.A. Custodio, R.E. Bretas, Thermal and structural characterization of nanofibers of poly (vinyl alcohol) produced by electrospinning, J. Appl. Polym. Sci. 112 (2009) 1680–1687.
[50] K.A. Khalil, H. Fouad, T. Elsarnagawy, F.N. Almajhdi, Preparation and characterization of electrospun PLGA/silver composite nanofibers for biomedical applications, Int. J. Electrochem Sci. 8 (2013) 3483–3493.
[51] S. Mollá, V. Compañ, Polyvinyl alcohol nanofiber reinforced Nafion membranes for fuel cell applications, J. Membr. Sci. 372 (2011) 191–200.
[52] J.E. Dunphy, K. Udupa, Chemical and histochemical sequences in the normal healing of wounds, N. Engl. J. Med. 253 (1955) 847–851.
[53] K.E. Espelie, V.R. Franceschi, P. Kolattukudy, Immunocytochemical localization and time course of appearance of an anionic peroxidase associated with suberization in wound-healing potato tuber tissue, Plant Physiol. 81 (1986) 487–492.
[54] H.A. Stefanacci, D.K. Vandevender, R.L. Gamelli, The use of free tissue transfers in acute thermal and electrical extremity injuries, J. Trauma Injury Infect. Crit. Care 55 (2003) 707–712.
[55] S. Gordon, S. Imam, R. Greene, Starch-based Plastics-measurement of Biodegradability, CRC Press, Boca Raton, 1996. Polymeric materials encyclopedia, 78857901.
[56] E.A. Bursali, S. Coskun, M. Kizil, M. Yurdakoc, Synthesis, characterization and in vitro antimicrobial activities of boron/starch/polyvinyl alcohol hydrogels, Carbohydr. Polym. 83 (2011) 1377–1383.
[57] L.T. Sin, W. Rahman, A. Rahmat, M. Mokhtar, Determination of thermal stability and activation energy of polyvinyl alcohol–cassava starch blends, Carbohydr. Polym. 83 (2011) 303–305.
[58] M.E. Gomes, V.I. Sikavitsas, E. Behravesh, R.L. Reis, A.G. Mikos, Effect of flow perfusion on the osteogenic differentiation of bone marrow stromal cells cultured on starch-based three-dimensional scaffolds, J. Biomed. Mater. Res. Part A 67 (2003) 87–95.
[59] H. Ismail, N.F. Zaaba, The mechanical properties, water resistance and degradation behaviour of silica-filled sago starch/PVA plastic films, J. Elastomers Plast. 46 (2014) 96–109.
[60] Y. Chen, X. Cao, P.R. Chang, M.A. Huneault, Comparative study on the films of poly (vinyl alcohol)/pea starch nanocrystals and poly (vinyl alcohol)/native pea starch, Carbohydr. Polym. 73 (2008) 8–17.
[61] N. Follain, C. Joly, P. Dole, C. Bliard, Properties of starch based blends. Part 2. Influence of poly vinyl alcohol addition and photocrosslinking on starch based materials mechanical properties, Carbohydr. Polym. 60 (2005) 185–192.
[62] M.G. Haugh, C.M. Murphy, F.J. O'Brien, Novel freeze-drying methods to produce a range of collagen–glycosaminoglycan scaffolds with tailored mean pore sizes, Tissue Eng. Part C Methods 16 (2009) 887–894.
[63] R. Gundle, K. Stewart, J. Screen, J.N. Beresford, Isolation and Culture of Human Bone-derived Cells, Cambridge University Press, Cambridge, 1998.
[64] T. Schmelzle, M.N. Hall, TOR, a central controller of cell growth, Cell 103 (2000) 253–262.